Supplemental Figure 1

A

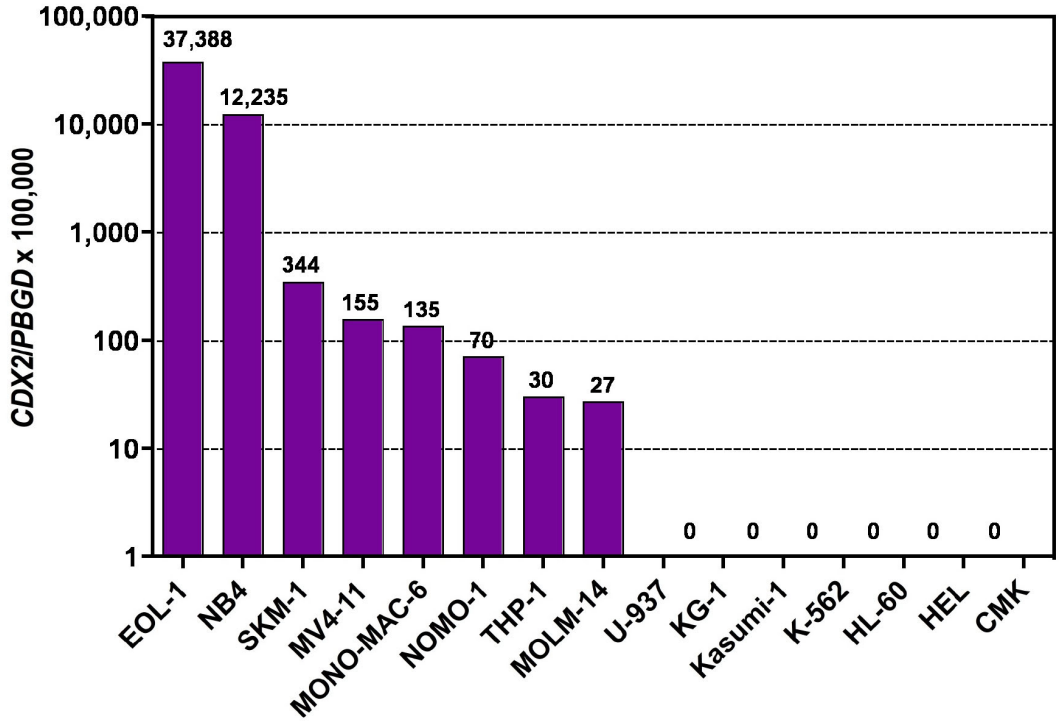

B

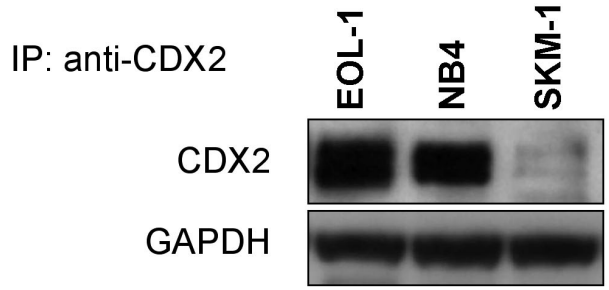

Supplemental Figure 2

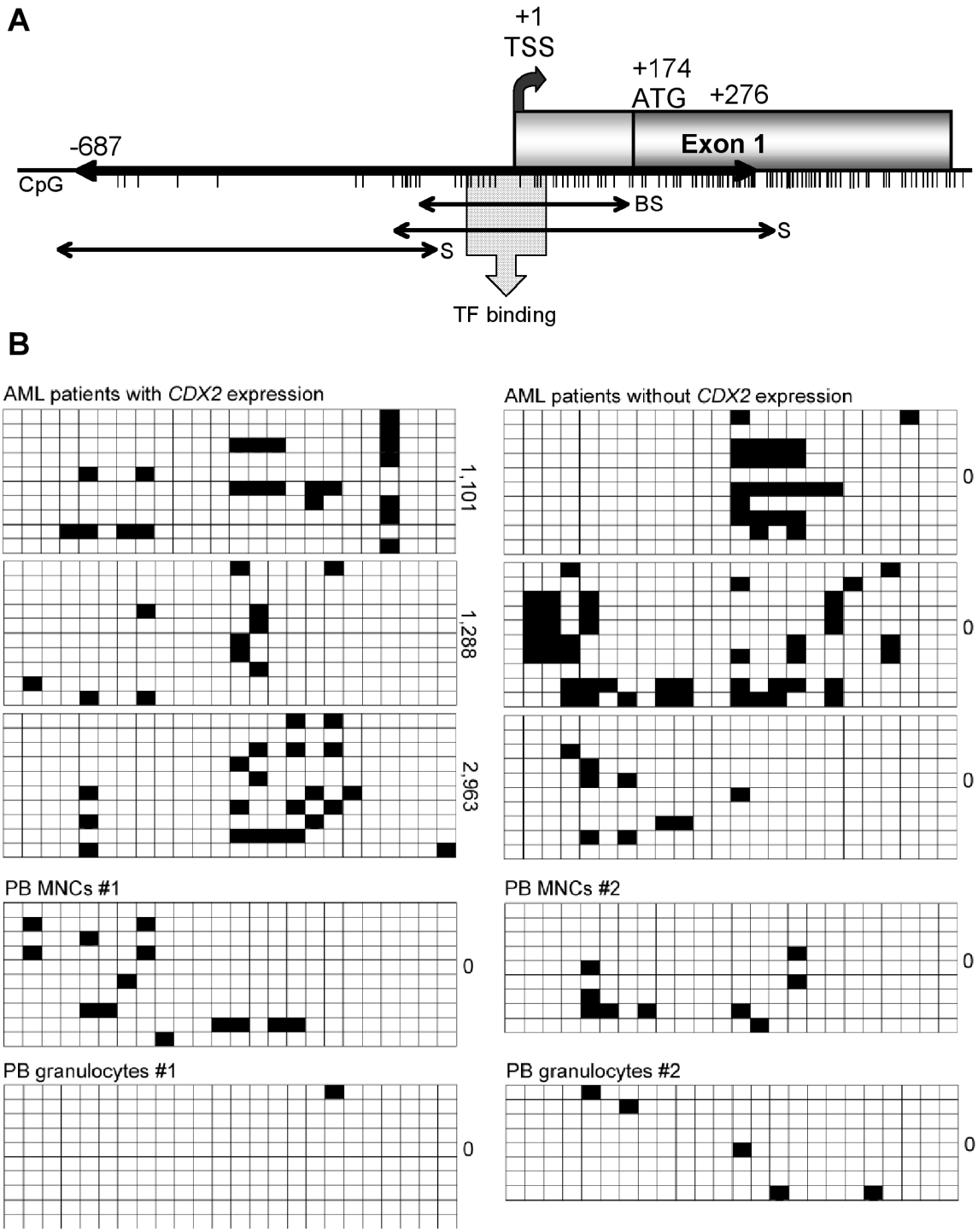

Supplemental Figure 3

A

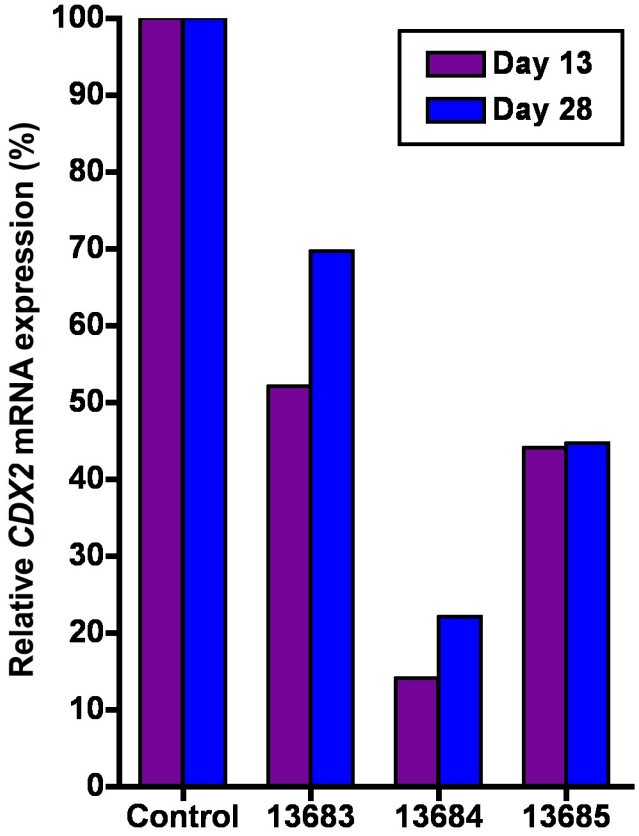

B

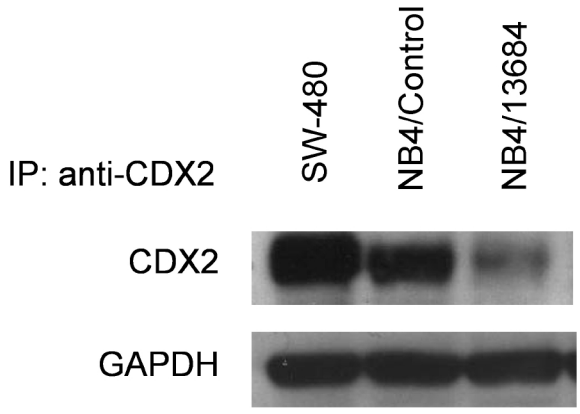

Supplemental Figure 4

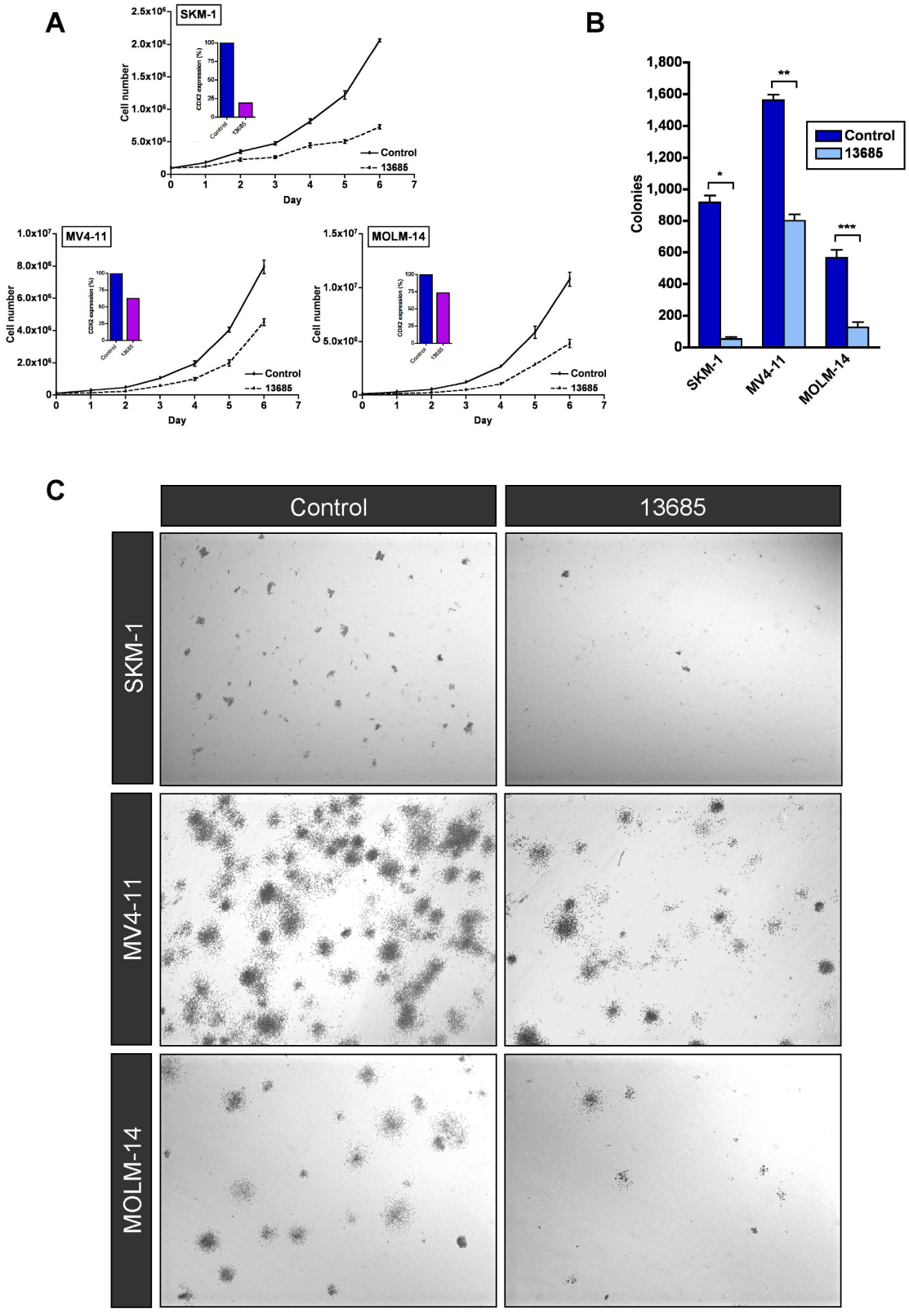

Supplemental Figure 5

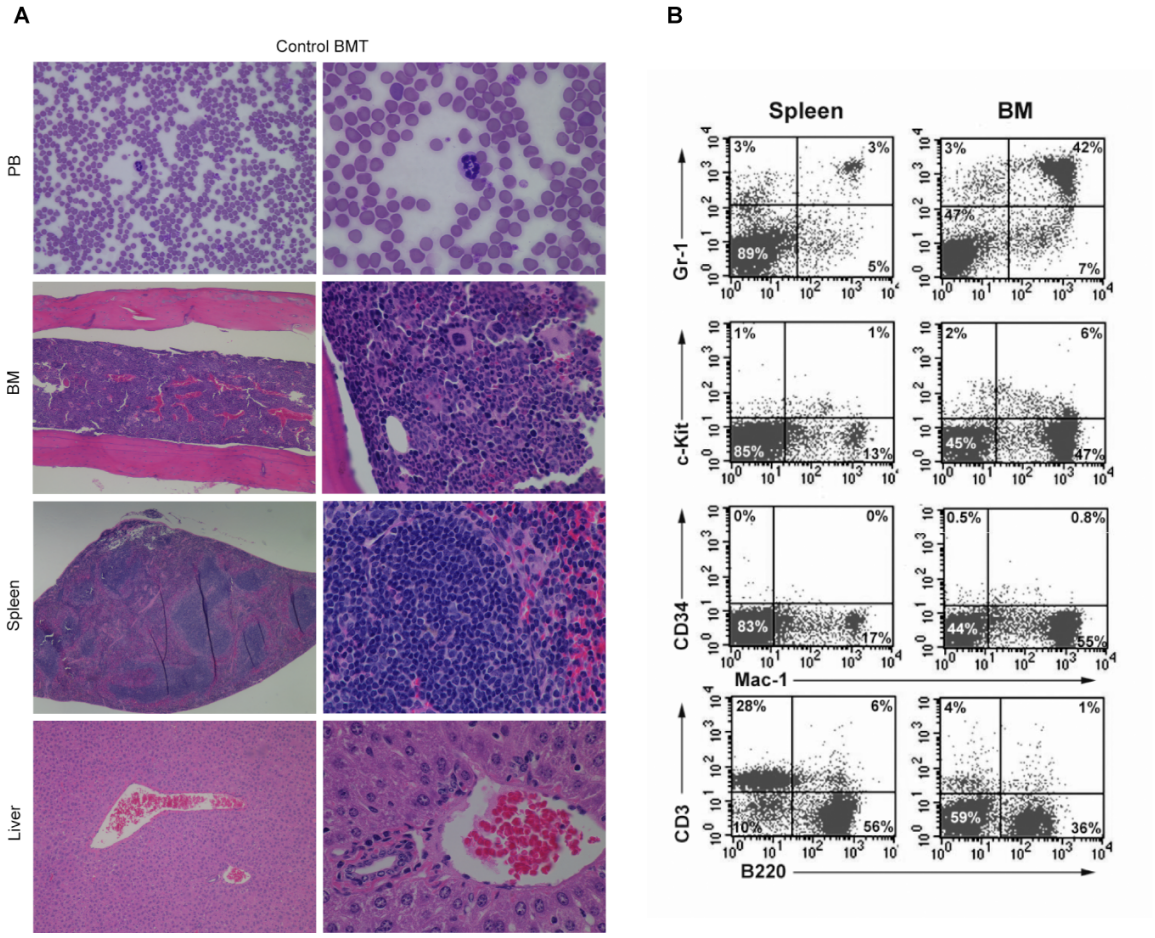

Supplemental Figure 6

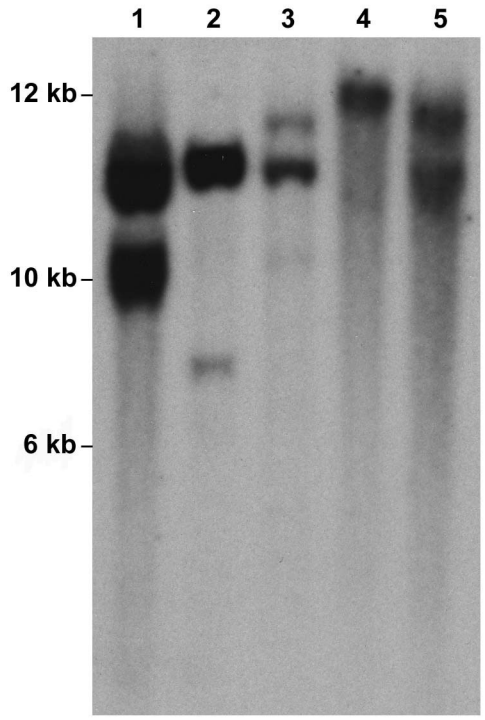

Supplemental Figure 7

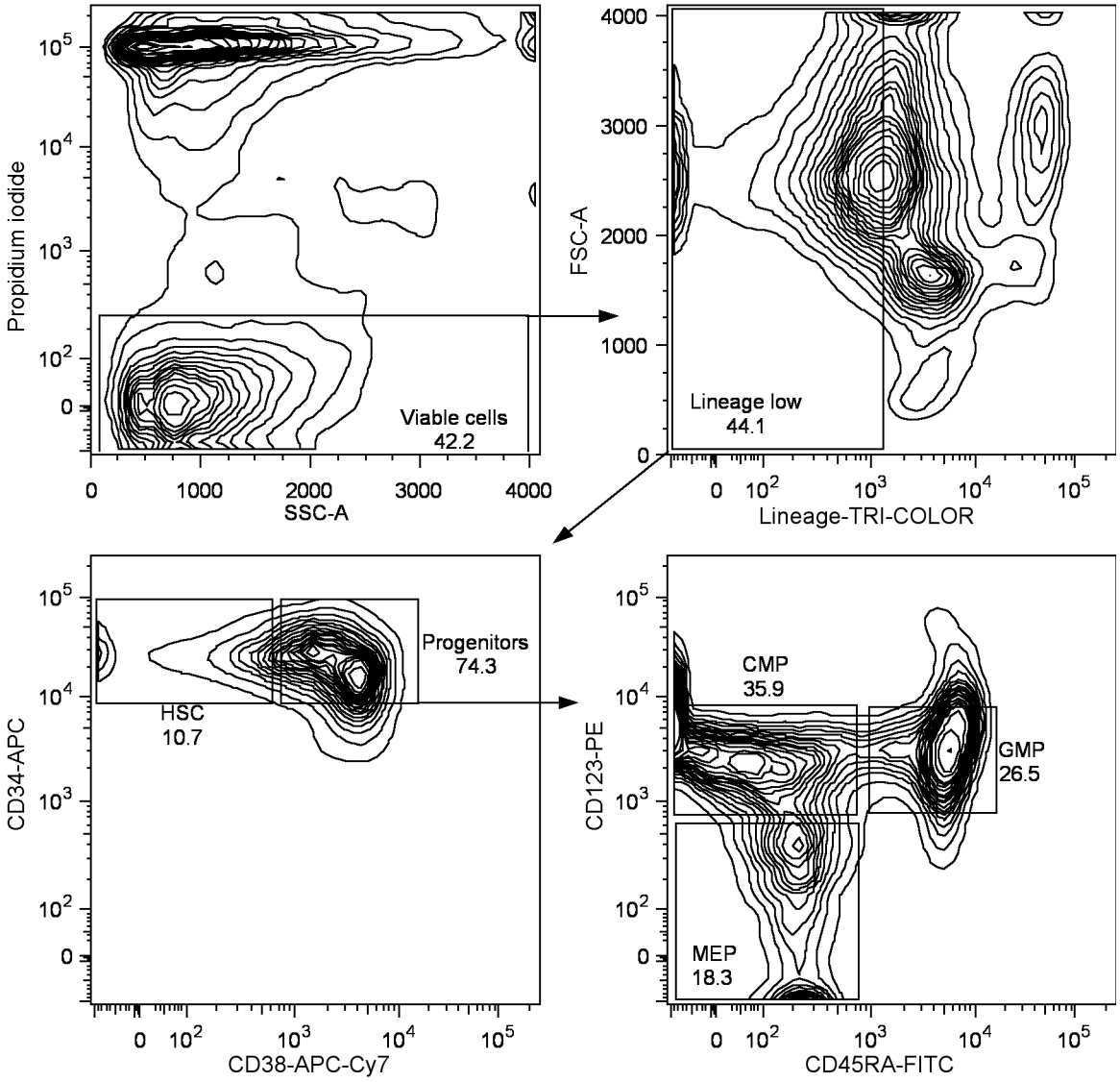

Supplemental Figure 1

CDX2 expression in human myeloid leukemia cell lines. **(A)** *CDX2* mRNA levels were measured by RQ-PCR in 14 AML cell lines and the CML cell line K-562. **(B)** Analysis of selected AML cell lines by immunoblotting showed varying CDX2 protein levels that correlated with *CDX2* mRNA levels. CDX2 was immunoprecipitated from whole-cell lysates, and immunoprecipitates were analyzed by Western blotting. To control for equal loading of proteins, aliquots of the lysates were analyzed by Western blotting using anti-GAPDH (FL-335; Santa Cruz Biotechnology). The two bands represent the phosphorylated and nonphosphorylated forms of CDX2.

Supplemental Figure 2

Methylation status of the *CDX2* promoter in AML. **(A)** The predicted proximal promoter of human *CDX2* spans 687 nucleotides 5' of the annotated TSS and the first 276 nucleotides of exon 1. The approximate location of transcription factor (TF) binding sites that have been identified in the murine *Cdx2* promoter and individual CpG dinucleotides are indicated. BS, CpG island analyzed by sodium bisulfite sequencing; S, genomic region studied by DNA sequence analysis. **(B)** Sodium bisulfite sequencing showed that the CpG island in the 5'-flanking region of *CDX2* was predominantly unmethylated in BM MNCs from three *CDX2*-expressing AML patients (expression levels, 1,101; 1,288; and 2,963, respectively), BM MNCs from three *CDX2*-negative AML patients, and PB MNCs and granulocytes from two healthy individuals without detectable *CDX2* expression. For each sample, the methylation status of 24 CpG dinucleotides is shown.

Each row represents a single PCR clone. Methylated CpG dinucleotides are shaded. *CDX2* expression levels are shown next to each cluster of clones.

Supplemental Figure 3

Stable silencing of *CDX2* expression by lentivirus-delivered shRNA constructs. **(A)** Transduction of the NB4 cell line with three different shRNA constructs targeting *CDX2* resulted in decreased mRNA levels as compared to a control construct lacking a hairpin insert. The most potent effect was observed with shRNA TRCN13684 (86% mRNA knockdown), followed by TRCN13685 (56%) and TRCN13683 (48%). Quantification of *CDX2* mRNA 13 and 28 d after transduction gave similar results, indicating stable downregulation of *CDX2* expression. **(B)** Suppression of *CDX2* mRNA was associated with a substantial reduction in CDX2 protein. NB4 cells were transduced with the nonsilencing control construct or shRNA TRCN13684. After 28 d, CDX2 was immunoprecipitated from whole-cell lysates, and immunoprecipitates were analyzed by Western blotting. To control for equal loading of proteins, aliquots of the lysates were analyzed by Western blotting using anti-GAPDH (FL-335; Santa Cruz Biotechnology). The CDX2-expressing colon cancer cell line SW-480 (S1) was used as positive control.

Supplemental Figure 4

Proliferation and colony formation of AML cell lines after silencing of *CDX2* expression using an alternative shRNA. **(A)** Downregulation of *CDX2* expression by shRNA TRCN13685 inhibited proliferation of the *CDX2*-expressing AML cell lines SKM-1, MV4-11, and MOLM-14. For each of the cell lines, the degree of mRNA knockdown is

given in a bar chart (SKM-1, 81%; MV4-11, 38%; MOLM-14, 27%). Experiments were performed in triplicate. Values are represented as mean ± SEM. **(B)** Colony-forming assays showed a significant reduction in the number of colonies for the *CDX2*-expressing cell lines SKM-1, MV4-11 (1×10^4 plated cells), and MOLM-14 (1×10^3 plated cells) after *CDX2* mRNA knockdown by shRNA TRCN13685 as compared to cells transduced with the nonsilencing control construct. Experiments were performed in duplicate. Values are represented as mean ± SEM. $^{*}P = 0.003$; $^{**}P = 0.005$; $^{***}P = 0.02$. **(C)** Microscopic analysis of colonies derived from shRNA-transduced cells (right panels) showed a decrease in the number of colonies and the number of cells per colony as compared to cells transduced with the nonsilencing control construct (left panels). Representative photomicrographs of methylcellulose cultures are shown. Original magnification x 20.

Supplemental Figure 5

Histopathologic and flow cytometric analysis of a representative control mouse transplanted with MSCV-IRES-GFP-tranduced BM cells. **(A)** Microscopic analysis demonstrated an unremarkable PB smear and normal BM, liver, and spleen sections with no evidence of leukemia or other abnormalities. Panels display Wright-Giemsa-stained PB smears and H&E-stained tissue sections. Original magnification x 400 and x 1,000 (PB); x 100 and x 600 (BM, liver); and x 40 and x 600 (spleen). **(B)** Flow cytometric analysis of BM and spleen cells demonstrated normal expression of Sca-1, CD34, c-Kit, Mac-1, Gr-1, CD3, and B220.

Supplemental Figure 6

Proviral integration and clonality of *Cdx2*-induced leukemias. Southern blot analysis of the leukemic cells from each of the five mice transplanted with BM cells expressing *Cdx2* confirmed proviral integration and indicated that the primary leukemias were clonal (lane 4) or oligoclonal (lanes 1, 2, 3, and 5). Blots were probed with *GFP* cDNA.

Supplemental Figure 7

Prospective isolation of human HSCs, CMPs, GMPs, and MEPs from normal BM MNCs using multiparameter flow cytometry and high-speed cell sorting. Representative flow cytometry profiles are shown.

Supplemental References

S1. Dang, L.H., et al. 2006. CDX2 has tumorigenic potential in the human colon cancer cell lines LOVO and SW48. *Oncogene*. **25**:2264–2272.